Optimization method for star tracker orientation in the sun-pointing mode

Geng Wang (王 赓)[1,2], Fei Xing (邢 飞)[1,2,*], Minsong Wei (卫旻嵩)[3], Ting Sun (孙 婷)[1,2], and Zheng You (尤 政)[1,2]

[1]*Department of Precision Instrument, Tsinghua University, Beijing 100084, China*
[2]*State Key Laboratory of Precision Measurement Technology and Instruments, Tsinghua University, Beijing 100084, China*
[3]*Department of Mechanical Engineering, University of California, Berkeley, CA 94720, USA*
**Corresponding author: xingfei@mail.tsinghua.edu.cn*

Received February 27, 2017; accepted April 28, 2017; posted online May 26, 2017

The star tracker, an optical attitude sensor with high accuracy, is widely used in satellites for attitude determination and control. However, it is susceptible to the sunlight and the earthlight for application on satellites in the sun-synchronous orbit. Therefore, the suppression of the sunlight and the earthlight is important for the star tracker. In this Letter, a vector model is proposed to describe the relationship among the Sun, the Earth, and the satellite body, and, based on the equations of the boundary curves, the vector areas free from the sunlight and the earthlight in the body coordinate system of the satellite are derived. Meanwhile, the installation orientation of the star tracker and the corresponding exclusion angle of the earthlight are optimized. The simulation results indicate that the optimization method for the installation orientation and the exclusion angle of the star tracker is accurate and effective.

OCIS codes: 120.4640, 120.6085, 280.4788, 290.2648.
doi: 10.3788/COL201715.081201.

The star tracker is an optical attitude sensor with extremely high accuracy, the structure of which is mainly composed of the baffle, the lens, the image detector, and the processing unit, and it has been widely used in satellites[1,2]. To realize attitude determination from the weak star captured by the image detector of the star tracker, the strong light from the Sun and the Earth, which is harmful to the star tracker, should be eliminated[3–5]. Moreover, the accuracy of the star tracker is related to the suppression of the sunlight and earthlight on the detector[6]. Therefore, the improper installation orientation of the star tracker and the exclusion angle design of the baffle will reduce the signal-to-noise ratio (SNR) and the accuracy, and it may even lead to the star tracker's failure[7].

Many methods have been proposed to reduce the interference from the sunlight and the earthlight to the star tracker, including optimizing the processing algorithm of the star image to improve the accuracy[8–10], adopting a big baffle to shield the strong light outside the field of view (FOV)[11–13], coating the black material to the star tracker to absorb the strong light[14,15], and optimizing the installation orientation of the star tracker to avoid the sunlight and the earthlight entering into the FOV of the star tracker directly[16–20]. Moreover, given that the relationship among the Sun, the Earth, and the satellite body is complex, the improper installation orientation will lead to the star tracker's failure at some time[21,22]. Therefore, the installation orientation of the star tracker is an important factor for satellite design. In the aspect of the orientation of the star tracker, the influence on the navigation precision caused by the installation azimuth of the star tracker has been widely analyzed; however, the interference from the sunlight and the earthlight has seldom been considered. Reference [17] considered the sunlight and earthlight; however, this method was not suitable for the multi-maneuver attitudes situation and did not analyze the orientation of the star tracker when the satellite was in the sun-pointing mode.

In this Letter, a vector model was proposed to analyze the vector position of the sunlight and the earthlight in the body coordinate system of the satellite, which operates in the sun-synchronous orbit. Based on this model, the equations of the boundary curves of the earthlight were derived when the satellite was in the sun-pointing mode, and the vector areas not affected by the sunlight and the earthlight could be determined. Meanwhile, the orientation of the star tracker and the corresponding exclusion angle of the earthlight could be optimized. This method can not only optimize the installation orientation of the star tracker when the satellite is in the sun-pointing mode, but it can also obtain the exclusion angle of the earthlight and the sunlight.

For the sun-synchronous satellite, the relative position among the Earth, the satellite, and the Sun changes all the time, however, the right ascension difference between the ascending node and the mean sun is constant. Meanwhile, the angle between the sun light and the orbit plane periodically changes with a small variance. Therefore, we can concisely describe aforementioned relative position based on the body coordinate system of the satellite.

In this vector model, the complex rotation relationship among the Sun, the Earth, and the satellite is transformed

so that the Earth and the Sun rotate around the satellite; thus, we can obtain the vector areas that suffered the sunlight and the earthlight based on the body coordinate system of the satellite. It is well known that any spatial orientation can be represented by the vector [cos α, cos β, cos γ] at a certain time. Since the sunlight is parallel, it can be described by this model, where α, β, γ represent the angles between the vector and the X, Y, Z axis of the body coordinate system of the satellite, respectively. When the light rays come from all directions in space, it will form a sphere with the radius of one, as shown in Fig. 1.

For the sun-synchronous satellite, the Sun is simplified as a pointolite. However, the earthlight comes from a cone area with respect to the satellite, as shown in Fig. 2, where E_s donates the central line and V_a donates the generatrix, and the half angle of the cone δ_a can be roughly calculated with the equation below:

$$\delta_a = \arcsin[(E_r + d)/E_s], \tag{1}$$

where E_s denotes the distance between the satellite and the geocenter, E_r is the radius of the Earth, and d is the thickness of the atmosphere.

In order to achieve enough energy, when the satellite is not under the remote imaging mode, the normal direction of the solar panels should always point to the Sun. However, for some small remote sensing satellites, their solar panels cannot rotate relatively to the satellite body. For these satellites, the satellite surface with the solar panels should always point to the Sun. In this Letter, when the satellite is in the nadir-pointing mode, the X axis of the body coordinate system of the satellite points to the direction of movement, and the Z axis always points to the Earth, as shown in Fig. 3(a). Similarly, when the satellite is in the sun-pointing mode, the X axis of the body coordinate system of the satellite points in the direction of the Sun all of the time, as shown in Fig. 3(b).

In this case, the satellite has two operation modes and is equipped with the orbit control device, with the orbital altitude of 535 km and the local time of the descending node of 10:30. According to Eq. (1), when E_r is 6378 km and d is 100 km, δ_a is 69.57°. The influence from the sunlight and the earthlight when the satellite is in the sun-pointing mode can be analyzed, and the optimal orientation of the star tracker and the exclusion angle of the baffle can be determined in the following analysis.

When the satellite is in the sun-pointing mode, since the X axis always points to the direction of the sun, the sunlight is a vector along the $+X$ axis in the attitude sphere model all of the time, as shown in Fig. 4, and it has nothing to do with the orbit altitude and the local time of the descending node.

When the satellite is in the sun-pointing mode, the influence from the sunlight is straightforward; however, the influence from the earthlight is more complex. In this part, we simulated the relationship between the Earth–satellite vector and the body coordinate system of the satellite by the satellite tool kit (STK) for three years in orbit flight and extracted the equations of the boundary curves of the Earth–satellite vectors. Since the satellite had the orbit control device, the orbit parameters of the satellite were

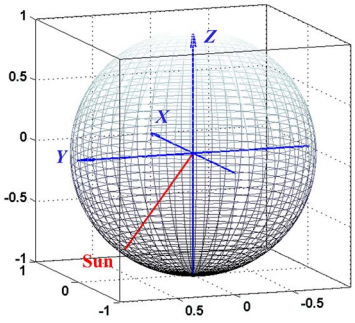

Fig. 1. Attitude sphere model of the sunlight based on the body coordinate system of the satellite.

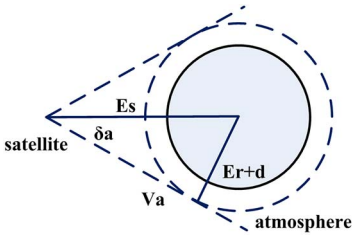

Fig. 2. Model of the earthlight for the sun-synchronous orbit satellite.

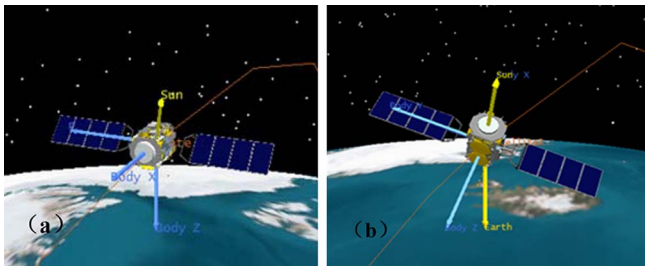

Fig. 3. (a) Nadir-pointing and (b) sun-pointing mode of the satellite.

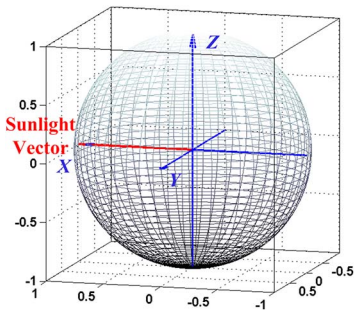

Fig. 4. Sunlight vector in the body coordinate system of the satellite.

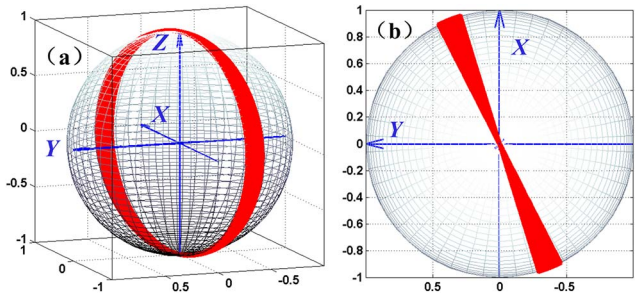

Fig. 5. (Color online) Earth–satellite vector area in the body coordinate system of the satellite, (a) three-dimensional (3D) view, (b) Z axis view.

constant. The simulation results are shown in Fig. 5, where the red area represents the Earth–satellite vector area during such a period, and the shape of the vector area is X from the Z axis view, as shown in Fig. 5(b). Moreover, the angles between the Earth–satellite vectors and the axes of the body coordinate system of the satellite during the period are listed in Table 1.

Based on the simulation results, the vector area can be expressed by two crossed boundary curves, as the view of Fig. 5(b), and the angles between the boundary curves and the axes of the coordinate system correspond to $X\_\min$ and $Y\_\min$. Therefore, the equations of the boundary curves can be derived, as expressed in

$$\begin{cases} x^2+y^2+z^2=1 \\ x=\tan(Y\_\min)\cdot y \end{cases}, \tag{2}$$

$$\begin{cases} x^2+y^2+z^2=1 \\ x=\tan(90^\circ - X\_\min)\cdot y \end{cases}, \tag{3}$$

which correspond to the boundary curves A and B in Fig. 6, respectively.

The earthlight is scattered light for the satellite in the sun-synchronous orbit. Based on the aforementioned analysis, the rotation boundaries of the earthlight can be derived from the boundary curves of the Earth–satellite vector area with factor δ_a, where δ_a equals 69.57°, as shown in

$$\begin{cases} x^2+y^2+z^2=1 \\ x=\tan(Y\_\min-\delta_a)\cdot y \end{cases}, \tag{4}$$

Table 1. Maximum and Minimum Angles Between the Coordinate Axes and the Earth–satellite Vector Area

Characteristics	Angle range
$X\_\min - X\_\max$	17.0791°–162.9209°
$Y\_\min - Y\_\max$	62.9930°–117.0135°
$Z\_\min - Z\_\max$	0°–180°

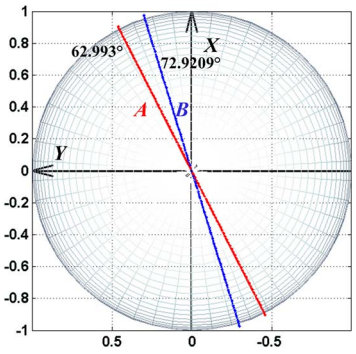

Fig. 6. Boundary curves of the Earth–satellite vector area.

$$\begin{cases} x^2+y^2+z^2=1 \\ x=\tan(90^\circ - X\_\min+\delta_a)\cdot y \end{cases}, \tag{5}$$

which correspond to curves C and D in Fig. 7, respectively.

The Earth–satellite vector rotates around the red area over time. Based on Eqs. (4) and (5), we can obtain the intersection point between the rotation boundary curves and the attitude sphere in the Z axis view. Thus, the equations of the boundary curves of the earthlight can be derived for this case, as shown in

$$\begin{cases} x^2+y^2+z^2=1 \\ x=\tan(Y\_\min)\cdot y \pm 2.0636 \end{cases}, \tag{6}$$

$$\begin{cases} x^2+y^2+z^2=1 \\ x=\tan(90^\circ - X\_\min)\cdot y \pm 3.1908 \end{cases}, \tag{7}$$

and Eq. (6) corresponds to curves E_1 and E_2, and similarly, Eq. (7) corresponds to curves F_1 and F_2 in Fig. 7.

Based on Eqs. (6) and (7), the areas free from the sunlight and the earthlight can be achieved, as shown in Fig. 8. The overlapping area between the red circle and the blue circle is the area free from the sunlight and the earthlight, and there are two areas symmetrically distributed along the Z axis. When the satellite is in the nadir-pointing mode, the sunlight is around Y axis, and area ② might be interfered with by the sunlight when the satellite is under a large maneuver situation. Therefore, compared with area ②, area ① is more suitable for the installation orientation of the star tracker.

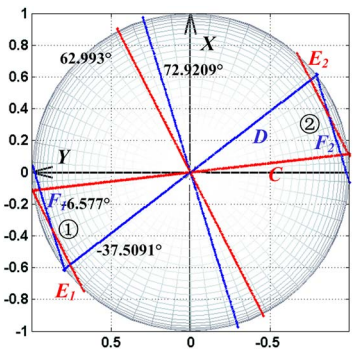

Fig. 7. Boundary curves of the earthlight in the Z axis view.

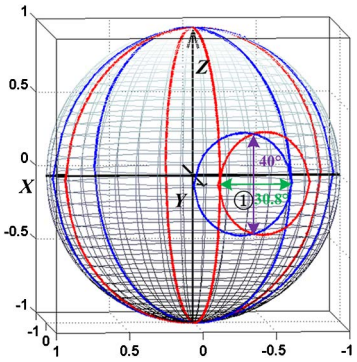

Fig. 8. Boundary curves of the Earth–satellite vector area.

As shown in Fig. 8, the angle range of area ① is about 30.8° along the XY plane, and the angle range along the Z axis is about 40°. Therefore, when the star tracker points to the center of area ①, we can get the maximum exclusion angle of the earthlight, which is about 15.4°.

In order to verify this method, we simulated the exclusion angle of the earthlight when the orientation of the star tracker was in the range of area ① by the STK. Since the period of the earthlight variation was one year, the simulation duration was set to be one year. Based on the aforementioned analysis, when the orientation of the star tracker is in the center of area ①, the exclusion angle can reach the maximum, as shown in Fig. 9, and the orientation parameters of the star tracker are shown in Table 2.

As shown in Fig. 9, the purple arrow is the orientation of the star tracker. In this case, if this method is effective, the exclusion angle of the earthlight plus the half angle of cone δ_a should be greater than 84.97°. The simulation result is shown in Fig. 10, where the minimum angle between the orientation of the star tracker and the Earth–satellite vector is greater than 84.97° during that period, and, therefore, the simulation results have validated the analysis.

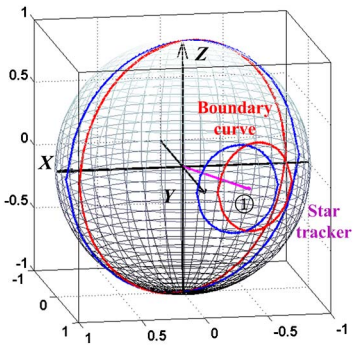

Fig. 9. Installation orientation of the star tracker.

Table 2. Installation Orientation of the Star Tracker in Sun-pointing Mode

	X	Y	Z
Angle between the star tracker orientation and axis of the coordinate system	112°	22°	90°

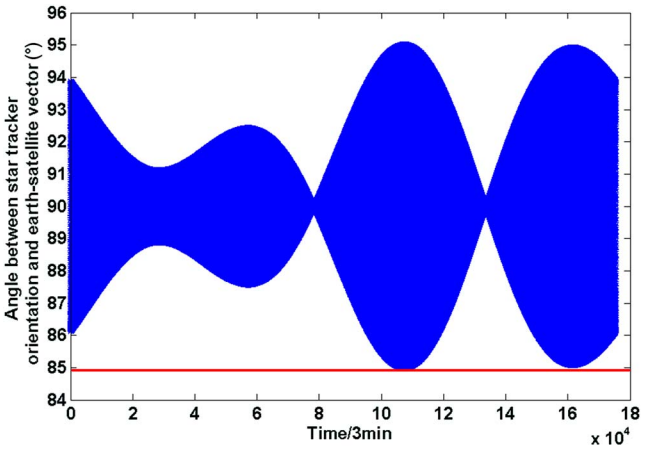

Fig. 10. Angle between star tracker orientation and the Earth–satellite vector for one year.

In this Letter, a novel method for the installation orientation of the star tracker is proposed when the satellite is in the sun-pointing mode. The area of the Earth–satellite vector is determined based on the attitude sphere model, which can describe the relative position among the Sun, the Earth, and the satellite body, and the equations of the boundary curves of the Earth–satellite area are derived. Moreover, the equations of earthlight boundary curves are calculated based on the relationship between the earthlight and the satellite, and the vector areas free from the earthlight and sunlight are determined during the period at the same time. Based on the vector area free from the earthlight and the sunlight, the pointing orientation of the star tracker is optimized. The simulation results indicate that the angles between the star tracker orientation and the earthlight are consistent with the design, and this method can effectively solve the installation orientation problem of the star tracker when the satellite is in the sun-pointing mode.

This work was supported by the State Key Laboratory of Precision Instrument Measurement, Tsinghua University under the financial support of the National Natural Science Foundation of China (NSFC) (Nos. 61377012, 51522505, 61605099, and 61505094).

References

1. C. C. Liebe, IEEE Aerosp. Electron. Syst. Mag. **10**, 10 (1995).
2. C. C. Liebe, IEEE Trans. Aerosp. Electron. Syst. **38**, 587 (2002).
3. J. L. Jørgensen, T. Denver, M. Betto, and P. Van den Braembussche, Acta Astronaut. **56**, 153 (2005).
4. J. Enright, D. Sinclair, C. Grant, G. McVittie, and T. Dzamba, in *Small Satellite Conference* (2010).
5. Z. Li, H. Lu, and X. Yuan, Chin. Opt. Lett. **13**, 111101 (2015).
6. D. Michaels and J. Speed, in *2005 IEEE Aerospace Conference* (2005), p. 1.

7. T. Dzamba, J. Enright, D. Sinclair, K. Amankwah, R. Votel, I. Jovanovic, and G. McVittie, in *Proceedings from 28th Annual AIAA/USU Conference on Small Satellites* (2014).
8. T. Sun, F. Xing, Z. You, and M. Wei, Opt. Express **21**, 20096 (2013).
9. T. Sun, F. Xing, X. Wang, Z. You, and D. Chu, Sci. Rep. UK **6**, 22593 (2016).
10. H. Zhou and Y. Yu, Chin. Opt. Lett. **14**, 121501 (2016).
11. J. P. Arnoux, Proc. SPIE **2864**, 333 (1996).
12. H. Kawano, H. Shimoji, S. Yoshikawa, K. Miyatake, K. Hama, and S. Nakamura, Opt. Eng. **45**, 124403 (2006).
13. J. A. P. Leijtens, "Star Tracker with Baffle," U.S. patent 8,249,809 (August 12, 2012).
14. S. H. McCall, S. M. Pompea, R. P. Breault, and N. L. Regens, Proc. SPIE **1753**, 158 (1993).
15. Y. S. Lee, Y. H. Kim, Y. Yi, and J. Kim, J. Korean Astron. Soc. **33**, 165 (2000).
16. F. Jiancheng and N. Xiaolin, IEEE Trans. Instrum. Meas. **58**, 3576 (2009).
17. L. Zhao, Z. Su, and Y. Hao, Transducer Microsyst. Technol. **12**, 9 (2013).
18. R. Vaughan and D. O'shaughnessy, in *AIAA Guidance, Navigation and Control Conference and Exhibit* (2008), p. 7479.
19. G. Wang, F. Xing, M. Wei, and Z. You, Appl. Opt. **54**, 10467 (2015).
20. M. Wei, F. Xing, Z. You, and G. Wang, Opt. Express **22**, 23094 (2014).
21. L. Blarre, J. Ouaknine, L. Oddos-Marcel, and P. E. Martinez, in *AIAA Guidance, Navigation, and Control Conference and Exhibit* (2006).
22. E. van Breukelen, in *Proceedings of the 60th International Astronautical Congress* (2009), p. 12.